ELSEVIER

Astroparticle Physics 6 (1997) 113–128

Astroparticle Physics

The performance of MACRO liquid scintillator in the search for magnetic monopoles with $10^{-3} < \beta < 1$

MACRO Collaboration

M. Ambrosio [l,*], R. Antolini [g], G. Auriemma [n,l], R. Baker [k], A. Baldini [m], G.C. Barbarino [l], B.C. Barish [d], G. Battistoni [f,2], R. Bellotti [a], C. Bemporad [m], P Bernardini [j], H. Bilokon [h], V. Bisi [q], C. Bloise [f], T. Bosio [i], C. Bower [h], S. Bussino [n], R. Cafagna [a], M. Calicchio [a], D. Campana [l], M. Carboni [f], M. Castellano [a], S. Cecchini [b,3], F. Cei [m,4], V. Chiarella [f], A. Corona [n], S. Coutu [k], G. De Cataldo [a], H. Dekhissi [b,5], C. De Marzo [a], I. De Mitri [i], M. De Vincenzi [n,6], A. Di Credico [g], O. Erriquez [a], R. Fantini [b], C. Favuzzi [a], C. Forti [f], P. Fusco [a], G. Giacomelli [b], G. Giannini [m,7], N. Giglietto [a], M. Goretti [n], M. Grassi [n], P. Green [p,8], A. Grillo [g], F. Guarino [l], P. Guarnaccia [a], C. Gustavino [g], A. Habig [h], K. Hanson [k], A. Hawthorne [h], R. Heinz [h], J.T. Hong [c], E. Iarocci [f,9], E. Katsavounidis [d], E. Kearns [c], S. Kyriazopoulou [d], E. Lamanna [n], C. Lane [e], D.S. Levin [k], P. Lipari [n], G. Liu [d], R. Liu [d], N.P. Longley [o], M.J. Longo [k], G. Ludlam [c], G. Mancarella [j], G. Mandrioli [b], A. Margiotta-Neri [b], A. Marini [f], D. Martello [j], A. Marzari-Chiesa [q], M.N. Mazziotta [a], D.G. Michael [d], S. Mikheyev [g,10], L. Miller [h], P. Monacelli [i], T. Montaruli [a], M. Monteno [q], S. Mufson [h], J. Musser [h], D. Nicoló [m,4], R. Nolty [d], C. Okada [c], C. Orth [c], G. Osteria [l], O. Palamara [j], S. Parlati [g], V. Patera [f,8], L. Patrizii [b], R. Pazzi [m], C.W. Peck [d], S. Petrera [j], N.D. Pignatano [d], P. Pistilli [j], V. Popa [b,11], A. Rainó [a], J. Reynoldson [g], F. Ronga [f], U. Rubizzo [b,3], A. Sanzgiri [p], F. Sartogo [n], C. Satriano [n,l], L. Satta [f,8], E. Scapparone [g], K. Scholberg [d], A. Sciubba [f,8], P. Serra-Lugaresi [b], M. Severi [n], V. Sinev [m,12], M. Sitta [q], P. Spinelli [a], M. Spinetti [f], M. Spurio [b], R. Steinberg [e], J.L. Stone [c], L.R. Sulak [c], A. Surdo [j], G. Tarlé [k], V. Togo [b], V. Valente [f], C.W. Walter [d], R. Webb [p]

[a] *Dipartimento di Fisica dell'Università di Bari and INFN, 70126 Bari, Italy*
[b] *Dipartimento di Fisica dell'Università di Bologna and INFN, 40126 Bologna, Italy*
[c] *Physics Department, Boston University, Boston, MA 02215, USA*
[d] *California Institute of Technology, Pasadena, CA 91125, USA*
[e] *Department of Physics, Drexel University, Philadelphia, PA 19104, USA*
[f] *Laboratori Nazionali di Frascati dell'INFN, 00044 Frascati, Roma, Italy*
[g] *Laboratori Nazionali del Gran Sasso dell'INFN, 67010 Assergi, L'Aquila, Italy*

PII S0927-6505(96)00048-5

[h] Department of Physics and Department of Astronomy, Indiana University, Bloomington, IN 47405, USA
[i] Dipartimento di Fisica dell'Università dell'Aquila and INFN, 67100 L'Aquila, Italy
[j] Dipartimento di Fisica dell'Università di Lecce and INFN, 73100 Lecce, Italy
[k] Department of Physics, University of Michigan, Ann Arbor, MI 48109, USA
[l] Dipartimento di Fisica dell'Università di Napoli and INFN, 80125 Napoli, Italy
[m] Dipartimento di Fisica dell'Università di Pisa and INFN, 56010 Pisa, Italy
[n] Dipartimento di Fisica dell'Università di Roma 'La Sapienza' and INFN, 00185 Roma, Italy
[o] Swarthmore College, Department of Physics and Astronomy, Swarthmore, PA 19081, USA
[p] Physics Department, Texas A & M University, College Station, TX 77843, USA
[q] Dipartimento di Fisica Sperimentale dell'Università di Torino and INFN, 10125 Torino, Italy

Received 5 June 1995; accepted 11 June 1996

Abstract

MACRO is designed to make a multiply redundant search for GUT magnetic monopoles over a wide velocity range. The 100 MHz pulse height recorder and synchronous encoder (PHRASE) and the energy reconstruction processor (ERP) are two components of that search, both based on the MACRO liquid scintillator. They are sensitive to monopoles with or without captured nuclei in the range $\beta \sim 10^{-3}$ to $\beta \sim 1$. Here, the performance of these systems is discussed, including also analysis methods and background evaluations.

1. Introduction

The possibility of isolated magnetic charges (magnetic monopoles) was discussed by Dirac [1] as early as 1931. 't Hooft, Polyakov and Preskill [2,3] showed that within the framework of grand unified theories (GUT's), magnetic monopoles emerge naturally from the symmetry breaking of the grand unified group into the strong and electroweak groups. It is possible that this occurred in the early stages of the big bang [4], producing a residue of primordial monopoles for which the GUT formalism predicts a mass on the order of 10^{16} to 10^{17} GeV/c^2.

Typical monopole velocities relative to the earth depend upon whether they are gravitationally bound to the solar system ($\beta \sim 10^{-3}$) or the galaxy ($\beta \sim 10^{-4}$) [5]. It may also be possible to accelerate magnetic monopoles to much higher velocities if supernova remnants, etc. are considered [6]. In any case, we assume an isotropic flux because the GUT monopole mass is so large that the stopping power of the earth can be neglected [7–9]. This is true whether the monopoles are bare or whether they have captured nuclei and the techniques described here are sensitive to both possibilities.

Redundancy and complementarity among separate detector systems are a central feature of the MACRO experiment. Because of the great importance which may be associated with any positive magnetic

* Corresponding author.
[1] Also Università della Basilicata, 85100 Potenza, Italy.
[2] Also INFN Milano, 20133 Milano, Italy.
[3] Also Istituto TESRE/CNR, 40129 Bologna, Italy.
[4] Also Scuola Normale Superiore di Pisa, 56010 Pisa, Italy.
[5] Also Faculty of Sciences, University Mohamed I, BP 424, Oujda, Morocco.
[6] Also Dipartimento di Fisica, Università di Roma Tre, Roma, Italy.
[7] Also Università di Trieste and INFN, 34100 Trieste, Italy.
[8] Sandia National Laboratory, Albuquerque, NM 87185, USA.
[9] Also Dipartimento di Energetica, Università di Roma, 00185 Roma, Italy.
[10] Also Institute for Nuclear Research, Russian Academy of Science, 117312 Moscow, Russia.
[11] Also Institute for Atomic Physics, 76900 Bucharest, Romania.
[12] Also Institute of General and Nuclear Physics, RRC Kurchatov Institute, 123183 Moscow, Russia.

monopole claim, MACRO includes several independent particle detection systems which provide multiple profiles of candidate events. Of these, the 100 MHz pulse height recorder and synchronous encoder (PHRASE) and energy reconstruction processor (ERP) are scintillator-based techniques useful in the velocity range $\beta \sim 10^{-3}$ to $\beta \sim 1$. These systems, complement the capability of MACRO to search for magnetic monopoles in a wide β range ($\beta > 10^{-4}$). In this paper we describe in detail the two scintillator-based systems suited for fast monopoles, including the discussion of the analysis methods. A preliminary work, mainly aimed to the evaluation of background, is also presented. The results of a search for slow monopoles using scintillators has been presented previously [13]. The discussion of the performance of the track-etch and streamer tube systems of MACRO in monopole detection has been published in [14,15].

2. The MACRO detector

The MACRO (Monopole, Astrophysics and Cosmic Ray Observatory) collaboration operates a large area underground detector [10,11] optimized to search for GUT magnetic monopoles from $\beta \sim 10^{-4}$ to $\beta \lesssim 1$. The design goal is for five years' exposure with sensitivity an order of magnitude below the Parker Bound, 10^{-15} cm^{-2} s^{-1} sr^{-1}, an upper limit on the monopole flux based upon the persistence of the interstellar magnetic field [12].

The MACRO detector is located in hall B of the *Laboratori Nazionali del Gran Sasso*, in the Abruzzo region of central Italy, with 3150 m water equivalent minimum overburden. The detector is composed of six adjacent supermodules, each of which is 12.6×12 m^2 with height 9.6 m. Including the enclosed steel support structure, the full detector measures 76.5×12 m^2 and 9.6 m high, with a total acceptance for isotropic flux of approximately 1.1×10^4 m^2 sr (Fig. 1). Each supermodule contains three distinct particle identification systems: liquid scintillation counters, 73% He–27% *n*-pentane gas-filled limited streamer tubes and Lexan/CR39 track etch detectors (Fig. 2). Here we focus on the ERP and PHRASE (scintillator) components of the long-term search for GUT magnetic monopoles and mention the other systems only briefly. More detailed descriptions are available in [10,11].

2.1. The liquid scintillation counters

The MACRO liquid scintillator system provides particle position, energy deposition and time-of-flight resolution of ≈ 11 cm, ≈ 1 MeV and ≈ 700 ps, respectively (for muons).

Each supermodule contains 49 horizontal and 28 vertical counters. The horizontal counters are grouped in three planes (bottom, central and top with 16, 16 and 17 counters respectively) and the verticals in two (east and west: 14 counters each). The bottom and center planes, along with the lower seven counters of the east and west planes, comprise the lower section of the supermodule; the top plane and upper seven counters of the east and west planes make up the upper parts of the 'attico'. Two additional vertical planes cover the lower sections (only) of the extreme north and south ends of the detector. This leaves the attico, which houses the readout electronics, open on the north and south faces (Figs. 1 and 2). In all there are 476 scintillation counters (294 horizontal and 182 vertical) with a total active mass of approximately 600 tons.

Horizontal scintillation counters measure 11.9×0.75 m^2 and 0.25 m in height and hold two photomultipliers at each end. Vertical counters measure 12.0×0.25 m^2 and 0.50 m in height, with one photomultiplier per end. All are filled with a scintillating mixture of 96.4% mineral oil and 3.6% pseu-

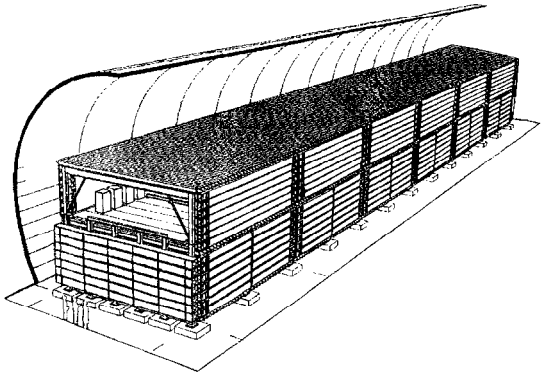

Fig. 1. The complete MACRO detector in perspective view. It is 76.5 m long, 12 m wide and 9.6 m high.

documene, with an additional 1.44 g/liter PPO and 1.4 mg/liter bis-MSB which act as wavelength shifters. The scintillator occupies a central sensitive region approximately 11 m long, while the endchambers containing the photomultipliers, focusing mirrors and associated electronics are filled with pure (nonscintillating) mineral oil. The nominal scintillator depths are 19 cm and 46 cm for the horizontal and vertical counters, respectively. Photomultiplier gain is maintained at approximately 5×10^6, for which a single photoelectron produces a most likely signal of ≈ 4 mV at the signal cable output.

2.2. The limited streamer tube and track etch detectors

Each supermodule also includes track etch and limited streamer tube detectors. The lower section includes ten horizontal streamer tube planes, alternating with the bottom and center scintillator counters and seven layers of passive rock absorber (420 g/cm^2 total rock thickness). The attico contains four additional streamer tube planes, two each on the top and bottom faces of the top scintillator plane. Vertical streamer tubes are arranged in twelve planes, four groups of three, which sandwich the east and west vertical scintillator planes. A similar arrangement covers the north and south (lower) scintillation counters. The limited streamer tubes provide particle tracking with resolution of $\approx 0.2°$ in angle and ≈ 1 cm in position.

The track etch detector is deployed in three separate sections: a horizontal plane near the middle of the lower section of the apparatus (just above the fifth streamer tube plane, see Fig. 2), a vertical plane covering the east face and a (smaller) vertical plane covering lower north face. The track etch system can be operated as a stand-alone detector or be 'triggered' by candidates in the streamer tube and/or scintillator systems. The CR39 component of the track etch has charge resolution of ≈ 0.2 e.

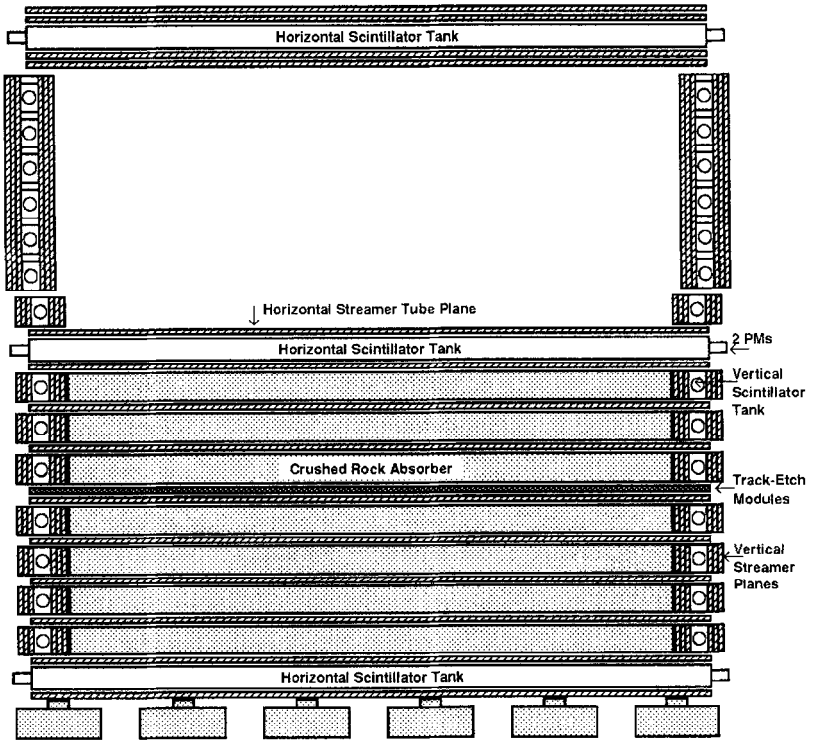

Fig. 2. A single MACRO supermodule in cross sectional view. It is 12.6 m long, 12 m wide and 9.6 m high.

3. Scintillator data acquisition

Scintillation light is collected using 20 cm hemispherical photomultipliers, EMI D642 and Hamamatsu R108, which employ a thirteen-stage fast venetian blind dynode structure. Signal risetimes are ≈ 10 ns with less than 1 ns jitter. Photomultiplier signals are transmitted via coaxial cable to one-to-one linear fanouts, which provide copies for the pulse height recorder and synchronous encoder (PHRASE), the energy reconstruction processor (ERP), the fast and slow monopole triggers (FMT and SMT, not discussed here), and the main waveform digitizer (WFD).

Two independent data acquisition (DAQ) systems are employed. The main DAQ is designed for monopole and rare particle searches and muon tracking, includes the streamer tubes, ERP, FMT, SMT and the main WFD. Three separate cpu's perform trigger and readout operations, each responsible for two of the six MACRO supermodules. The second DAQ, specifically designed for gravitational collapse neutrino detection, operates the PHRASE using an independent version of the same three- cpu readout configuration.

3.1. The energy reconstruction processor

The energy reconstruction processor (ERP) is a single-counter energy threshold trigger. It is the primary scintillator muon system, but includes a lower energy gravitational collapse (GC) neutrino trigger as well. ERP inter-counter timing is performed for times of flight of up to 400 ns; for longer times of flight the main WFD is used (Section 3.2). The ERP is sensitive to particles of any velocity that are capable of depositing the minimum trigger energy (≈ 8 MeV). The raw triggering efficiency for expected $\beta > 10^{-1}$ monopole signatures (the range of the ERP study) is essentially 100%.

An ERP trigger decision is requested when both ends of a single scintillation counter cross the front-end minimum bias threshold inside a 270 ns coincidence window. This threshold is adjusted on a counter-by-counter basis and ranges approximately from 50–150 mV. The actual trigger decision is made by comparing six-bit flash ADC evaluations of the two signal amplitudes to the energy values stored in a look-up table (LUT). If the result is above that counter's energy threshold, an ERP muon trigger is formed.

In addition to the trigger flash ADC, the ERP also employs a second-stage twelve-bit ADC which makes a more accurate photomultiplier pulse integration. This is applied to both the raw signal and a $10\times$ attenuated version, the latter being used for fast monopole analyses in which the nonattenuated ADC saturates. The ERP provides time of flight from TDC readout, calibrated weekly with delayed LED signals and variable-intensity laser pulses. Time walk effects, which cause pulses of different heights to reach TDC threshold at different relative times, are included.

3.2. The main waveform digitizer

In the ERP monopole analysis described here, MACRO employed LeCroy 2261 commercial waveform digitizers (WFD's). These were operated in 40 MHz (25 ns) common stop sampling mode with a 2 V dynamic range and an 8 μs recording window, providing time of flight for $\beta \sim 10^{-2}$ to $\beta \sim 10^{-1}$. Up to eightfold multiplexing was employed. In summer 1993 this system was replaced by a custom-designed 200 MHz, 64 kB zero-suppressed WFD with 10 V range which will be used in future analyses.

3.3. The PHRASE

The pulse height recorder and synchronous encoder (PHRASE) is a trigger and energy reconstruction system [10,11,16] designed to detect gravitational collapse neutrinos. It is therefore optimized for the study of low energy (~ 10 MeV or less) events. Its use can be extended, however, to the detection of other particles including magnetic monopoles. The energy-dependent trigger threshold is sensitive to the signals predicted for GUT monopoles in the range $\beta \sim 10^{-3}$ and above.

The PHRASE receives photomultiplier signals from both ends of the scintillation counter and provides a trigger when the energy deposition is larger than 7 MeV. The trigger signal is generated ≈ 40 ns after the average arrival time of the two pulses, which are recorded to ≈ 1 ns resolution. The PHRASE threshold is temporarily lowered to a sec-

ondary level of ≈ 1 MeV for 800 μs after each primary event.

The PHRASE WFD records photomultiplier signals from both ends of the triggering scintillation counter. Six-bit 100 MHz flash ADC's are used, with eight effective bits obtained by hyperbolic compression. Photomultiplier signals are recorded in an ~ 160 ns window centered on trigger formation, with the presence of a photomultiplier signal in either end of the counter beyond this time forcing additional readout in 160 ns intervals up to a maximum of 2.4 μs.

Because of the 7 MeV hardware energy threshold (which was optimized for collecting gravitational collapse events), a software cut of 10 MeV is applied in the monopole analysis. This is roughly one-third the energy loss expected for a typical cosmic ray muon. Signals at this level correspond to approximately 200 photoelectrons for a particle at the center of the counter; the nominal electronic trigger efficiency for such a signal is essentially 100% [16]. The PHRASE digitizer operates in free-running (zero dead time) mode using a 100 MHz base frequency, with approximately 99% efficient digitization. Comparison with independent PHRASE channels shows that this efficiency is independent of the relative arrival time of the signals and remains constant in a wide range of pulse heights.

4. Energy reconstruction issues

Bare GUT-type monopoles are assumed throughout the analyses described here, with energy losses and light emission given by Ahlen et al. [7–9]. MACRO sensitivity is, however, expected to include monopoles which have captured nuclei. Radiation quenching is taken into account via Birks' scintillator saturation formula [17] and the parameters measured for the MACRO scintillator. In addition, a recent measurement of the scintillation light emitted by protons may suggest a higher energy loss rate for monopoles in the region $\beta < 10^{-3}$ [18].

The visible energy loss functions $\mathrm{d}L/\mathrm{d}X$ (in MeV/cm) and $\Delta L/\Delta t$ (in MeV/10 ns) are plotted as a function of β in Fig. 3a and b. These plots show that the maximum expected monopole light output can be orders of magnitude above that produced by minimum ionizing particles, requiring energy loss measurements in the range $\beta > 10^{-3}$ to be accurate over a large dynamic range.

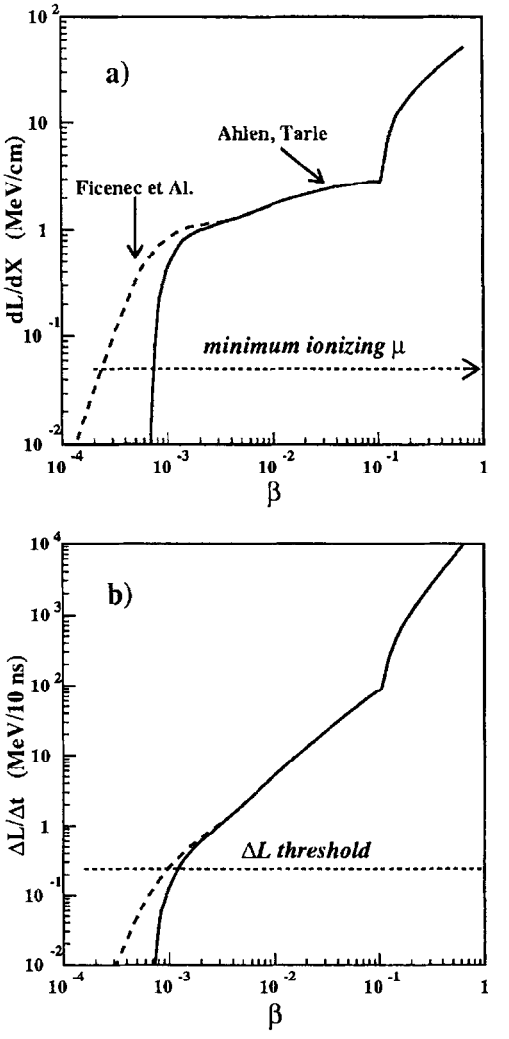

Fig. 3. Predicted monopole light yield in MACRO scintillator: (a) $\mathrm{d}L/\mathrm{d}X$ versus β, (b) $\Delta L/\Delta t$ versus β. The light yield is given as the calculated part of energy loss resulting in scintillation photon emission. The light output generated by a minimum ionizing cosmic ray muon and the PHRASE WFD threshold are also shown. The kink around $\beta = 10^{-1}$ corresponds to the onset of δ-ray production.

4.1. Scintillator and photomultiplier saturation

The scintillation light yield as a function of energy loss rate is given by Birks [17]

$$\frac{\mathrm{d}L}{\mathrm{d}X} = \frac{S(\mathrm{d}E/\mathrm{d}X)}{1 + B(\mathrm{d}E/\mathrm{d}X)}. \qquad (1)$$

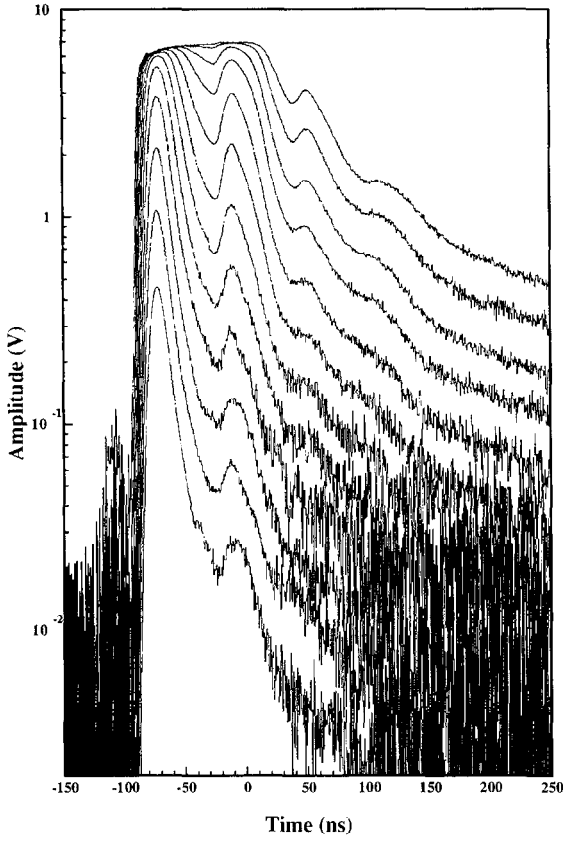

Fig. 4. Photomultiplier waveforms recorded at various laser light intensities. The first optical reflection is clearly visible. At higher intensities the second and third reflections become apparent, as do the effects of pulse saturation. A vertical muon corresponds to the pulse peaking at about 1 V.

Here dE/dX is the energy loss rate and dL/dX, S and B are the scintillation light yield, efficiency and saturation constant, respectively. The predicted yield for monopoles in MACRO scintillator can be calculated using the measured value of the saturation constant, $B = 11.6 \pm 0.06$ mg cm^{-2} MeV^{-1}. Even including this effect, however, the visible energy loss for $\beta \sim 10^{-3}$ monopoles remains more than one order of magnitude greater than that produced by minimum ionizing cosmic ray muons. This presents the possibility of photomultiplier saturation. The waveform deformation due to this effect is clearly visible in Fig. 4, which shows waveforms for a range of laser light intensities. Signal saturation effects become important at 2–3 × typical muon levels and are considered in both the ERP and PHRASE analyses (Sections 4.3 and 4.4).

4.2. The scintillator response function

Photomultiplier signals must be corrected to account for geometrical acceptance and light attenuation inside the scintillator. The net contribution of these two effects is determined by examining muon pulse heights. The most probable energy loss, obtained via a phenomenological fit to the pulse height distribution, taking into account the expected Landau shape folded with photoelectron statistics, is used to fix the absolute light deposition as a function of longitudinal position x. The result is the empirical scintillator response function (Fig. 5)

$$R(x) = \frac{a_1}{x^2} + a_2 e^{-x/a_3} + a_4 e^{-x/a_5}. \quad (2)$$

The parameters a_n quantify terms which can be interpreted as the inverse-square geometrical acceptance, attenuation within the scintillator and light losses at reflections from walls.

4.3. PHRASE energy reconstruction

The amount of energy deposited within the scintillator can be calculated by integrating the PHRASE

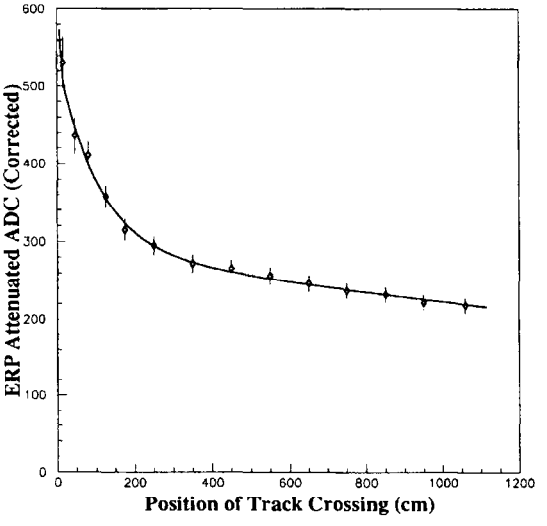

Fig. 5. The scintillator response function as measured by the ERP attenuated ADC. The signal is equivalent to that of a single cosmic ray muon passing vertically through a horizontal scintillation counter at the various longitudinal positions shown.

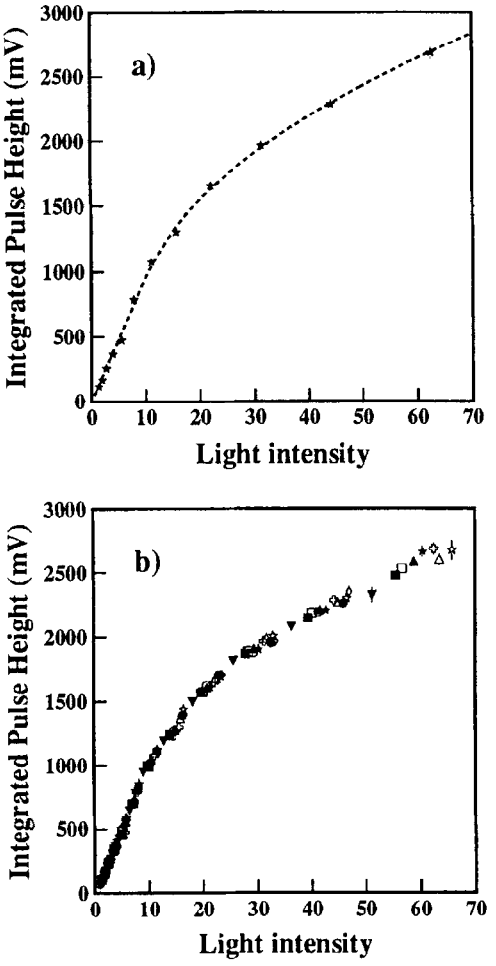

Fig. 6. The integrated PHRASE WFD signal as a function of calibration laser intensity (in arbitrary units). In (a) the functional fit is given; in (b) several normalized signals from different scintillation counters are compared.

waveform. Because the circuit was designed for low energy gravitational collapse physics, however, the saturation level is only 252 mV, which is typically obtained for $\approx$ 15 MeV deposited at the center of the counter. This causes the PHRASE flash ADC to saturate on most muon crossings ($\approx$ 30 MeV). Energy measurements at this level and above can still be made offline, however, because the base of the pulse becomes wider with increasing energy. The waveform integral thus increases monotonically (although nonlinearly) as a function of energy loss.

Fig. 6a shows the PHRASE response to MACRO nitrogen laser calibration pulses. In Fig. 6b signals from many different counters are compared (after normalization to account for differences in the fiber optic transmission lines and individual photomultiplier gains). The nonlinearity in the relationship between integrated pulse height and light intensity L (given here in arbitrary units) is due to the onset of flash ADC saturation; beyond this region, increases in energy deposition affect primarily the width rather than the height of the WFD signal.

Laser light, cosmic ray muons and natural gamma rays are all involved in the scintillator energy calibrations, but not all excite the same relative quantities of fast and slow scintillation light. This is shown in Fig. 7, which compares normalized laser and muon photomultiplier pulses. In addition to the main pulses, the first optical reflection is also visible (the time delay between the main pulse and the reflection is different for the two pulses because the light was emitted at different positions in the counter). Note that the muon pulse has a longer tail than the laser-induced pulse, an indication that ionizing radiation produces more of the slow scintillation component than the laser [17,19,20]. A dual exponential fit can

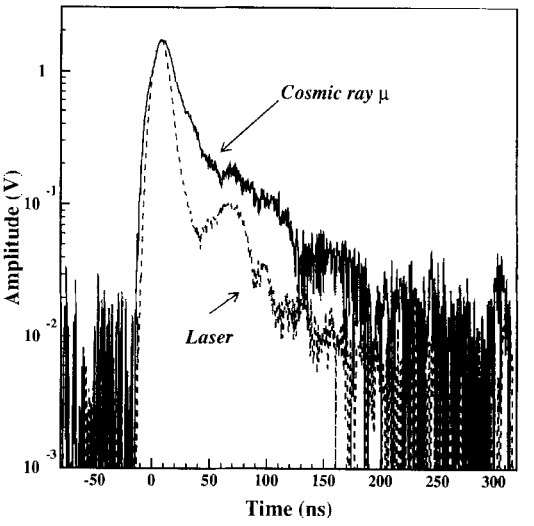

Fig. 7. Photomultiplier pulse shapes for laser and cosmic ray muon pulses (normalized). The muon pulse has a longer tail than the laser pulse, indicating additional excitation of the slow scintillation component. The first few optical reflections are also seen. The separation between the main and first reflected pulse is different for the two signals, which originated at different longitudinal positions.

be made to the muon pulse, giving time constants of $\tau_{fast} \approx 20$ ns and $\tau_{slow} \approx 60$–70 ns. Although exponential decay is a rough approximation for the complex time dependence of the slow component and the fit parameters are subject to significant systematic errors, the agreement is good.

The observed differences in pulse shape must be taken into account when comparing events generated by laser light and ionizing radiation. Since natural background radiation populates an energy loss region below that of interest to this analysis, however, the PHRASE response to very large pulses can only be indirectly measured with the laser calibration system. We have therefore adopted the following procedure in order to extrapolate event reconstruction to higher energies:

1. Photomultiplier signals from both cosmic ray muon and laser pulses are collected using a Tektronix TDS620 digital oscilloscope (2 GHz sampling rate) located at the input to the PHRASE WFD;
2. these photomultiplier pulses are Fourier transformed and filtered according to the hardware digitizer transfer function and the waveform at the PHRASE flash ADC is reconstructed from this signal by Fourier antitransform;
3. the two classes of pulse (muon and laser) are independently fit with Gaussian rise times and dual exponential tails, including optical reflections;
4. best-fit pulses are used to simulate flash ADC response to muon- and laser-induced events of all sizes; and, finally,
5. two different calibration functions relating pulse amplitude to integrated waveform are obtained, corresponding to muon and laser signals, respectively.

The laser calibration function was compared to direct PHRASE measures of laser events and found to closely reproduce the data as shown by the example of Fig. 6a. It is impossible to make the same comparison for the muon calibration function above the minimum ionizing particle regime, but, having accounted for the difference between laser and muon pulses, the muon calibration is assumed to correctly simulate PHRASE response up to extremely high energy losses.

Because the partition of scintillation light into fast and slow components could vary with ionization density, monopole light pulses might exhibit timing characteristics different from those of minimum ionizing particles. The PHRASE calibration might therefore lead to an overestimate of the real monopole energy loss. This possibility is accepted as part of a conservative approach to energy-based monopole studies.

The complete PHRASE energy reconstruction is as follows: integrated digital versions of the photomultiplier signals produced at each end of the triggering counter are independently corrected using the muon calibration and the scintillator response function (Eq. (2)), then normalized to account for differences in individual photomultiplier amplifications. This produces two independent measurements of event energy (one from each end of the tank), from which a weighted average is obtained.

Although the original PHRASE energy determination is made in arbitrary units, it is straightforward to

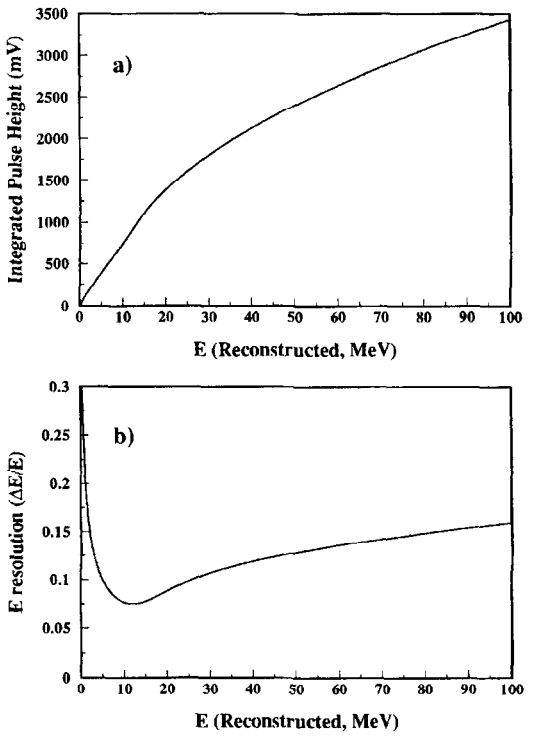

Fig. 8. The PHRASE response to ionizing radiation: (a) gives the functional relationship between integrated PHRASE WFD signal and energy deposition, (b) gives the resolution.

obtain the absolute energy scale from the ^{208}Tl 2.614 MeV gamma line and the known cosmic ray muon energy loss (≈ 30 MeV for a vertical crossing through a horizontal counter). An internal check on this reconstruction can be performed by calculating muon energies on the basis of the ^{208}Tl gamma alone; the difference between this calculation and the assumed muon energy deposition shows agreement within the nominal PHRASE energy resolution of approximately 10% at 30 MeV. Fig. 8a shows the functional relationship between integrated PHRASE WFD and energy deposition for events at the center of the counter; Fig. 8b shows the resolution.

4.4. ERP energy reconstruction

High energy ERP calibrations are performed on the $10\times$ attenuated ERP ADC's using the same nitrogen laser system employed by the PHRASE. The linear and higher energy nonlinear response regions are clearly seen in Fig. 9. Because the ERP attenuated ADC remains linear throughout the region considered here, the observed nonlinearity is due mainly to photomultiplier saturation. The straight region is fit according to

$$A = gL + P, \tag{3}$$

where A, g and P are the ERP attenuated ADC value, linear gain and pedestal, respectively; L is the relative laser light output. In order to accommodate the nonlinearity at higher light levels, L is fit according a fourth-order quadratic

$$L = b_0 + b_1 A + b_2 A^2 + b_3 A^3 + b_4 A^4, \tag{4}$$

where the b_n's are empirical fit constants and A is the pedestal-adjusted signal amplitude. Eq. (4) accounts for both photomultiplier and scintillator saturation so that the resultant light output L can be used in the linear response function (Eq. (3)). After adjusting for the position of the event via the scintillator

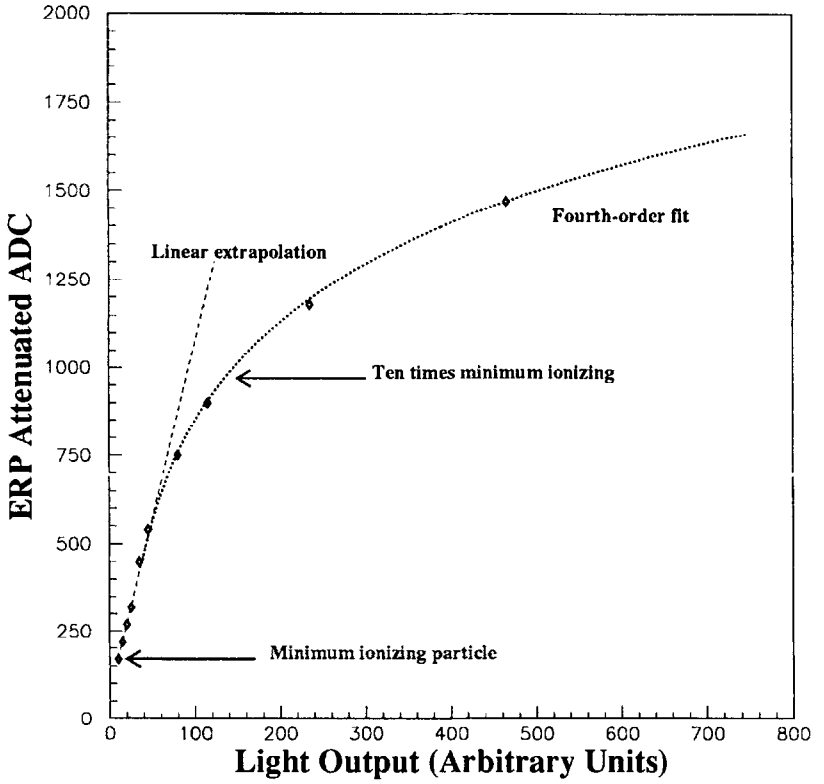

Fig. 9. The ERP attenuated ADC response to laser light with linear and fourth-order fits. The single and ten-times minimum ionizing particle levels are shown (for vertical tracks in a horizontal scintillation counter).

response function (Eq. (2)), the nominal energy-equivalent light output is determined according to Eq. (4). Because the ERP analysis does not account for the difference between laser- and muon-induced pulse shapes, it might overestimate the energy loss of a real monopole (Section 4.3) Although this issue is to be examined in more detail in future ERP studies, it is accepted as a more conservative contribution to the present analysis. Absolute energy calibration for the ERP, which is not sensitive to the ^{208}Tl gamma, is performed on the basis of muon data alone. The ADC value corresponding to the most probable single minimum ionizing particle is obtained from the peak of the Landau distribution. In the region typical of cosmic ray muon events (≈ 30 MeV), the net uncertainty in energy reconstruction is approximately 4%. At increasing energies this uncertainty becomes dominated by the saturation correction and approaches 10% at 2 GeV, the energy corresponding to the highest intensity laser light calibrations. Energy reconstructions are extrapolated to higher energies with about 20% uncertainty, but eventually the algorithm breaks down because the ERP ADC signal reaches a maximum when the length of the saturated photomultiplier pulse exceeds the integration gate width. While the energy corresponding to this maximum varies from counter to counter, we apply the most conservative (worst single counter case) upper limit of 8 GeV. Fig. 10a shows the reconstructed energy as a function of attenuated ADC, while Fig. 10b gives the relative uncertainty.

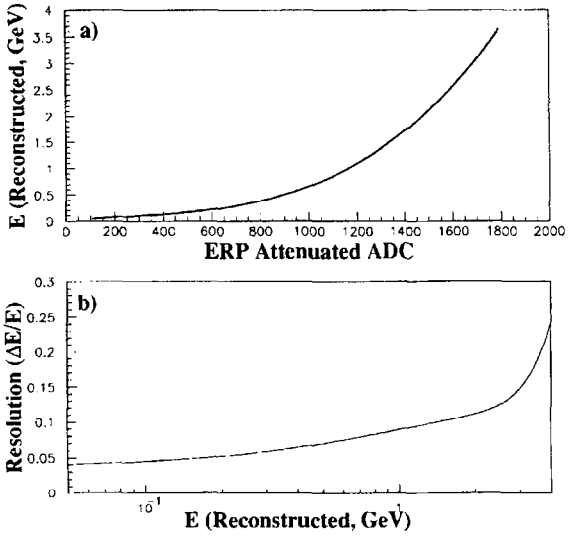

Fig. 10. The ERP attenuated ADC response to ionizing radiation, with the functional form in (a) and the relative energy resolution in (b).

4.5. Scintillator light reflections

The properties of the MACRO scintillation counters allow an alternative and original approach to achieving a large dynamic range: the optical reflection method. The MACRO light collectors produce optical reflections of approximately 5–10% of the incident intensity. The PHRASE photomultiplier waveforms show a corresponding sequence of pulses with decreasing amplitude (the signals appear ≈ 62, 124, 186... ns after the main pulse for an original signal at the center of the counter). The study of the waveforms in successive time slices corresponds therefore to the study of the event energy loss for a range of signal amplifications. Even though the light level associated with a very fast monopole would be so high as to saturate the photomultiplier and/or signal circuitry, such an event could still be studied in the unsaturated regime through the lower level signals associated with its successive reflections. At least one of these remains well within the linear dynamic range of the photomultiplier electronics and all are separated in time from the main signal and from the other optical reflections.

These optical reflections are visible in Fig. 4, as is waveform deformation due to photomultiplier saturation. As the pulses fall below the saturated region, they exhibit an undistorted pulse shape. This can be verified by renormalizing the photomultiplier pulses according to the known laser light intensities, which shows that the unsaturated regions agree.

5. Data collection and analysis

Data discussed here involve two of the individual contributions to the fully redundant MACRO monopole program, which also includes additional scintillator systems, the track etch detector and the streamer tubes. These data were collected from October 1989 to July 1993, during which time the upper section of the MACRO detector (the attico) had not yet become fully operational, so only the lower section is considered. These analyses apply to veloci-

ties of $1.2 \times 10^{-3} < \beta < 10^{-1}$ (the PHRASE) and $10^{-1} < \beta < 1$ (the ERP).

5.1. The PHRASE analysis

The PHRASE analysis includes two distinct data sets. The first (sample 1) was collected during the twenty-nine months from October 1989 to March 1992, using only the horizontal scintillator planes of the first supermodule, an exposure of 1.8×10^{14} cm^2 s sr. The second (sample 2) was acquired from December 1992 to June 1993 using the full lower section of all six supermodules (less the north and south faces), an exposure of 3.9×10^{14} cm s sr. Losses due to detector-wide hardware failures account for about 5% of the total data; in addition, certain individual channels are excluded due to localized electronics downtime. There is no surviving monopole candidate in the range $1.2 \times 10^{-3} < \beta < 10^{-1}$.

5.1.1. PHRASE event selection

Primary event selection is defined in the hypothesis of a single particle crossing the apparatus. It requires two hits in two different scintillator planes, each of them occupying a maximum of three adjacent counters. The spatial distance D between hits and the apparent particle velocity β are reconstructed from scintillation counter timing. The following cuts are applied:

1. The separation D is required to be at least 2 m in order to allow accurate time-of-flight and velocity reconstructions;
2. the velocity is restricted to $\beta < 10^{-1}$ in order to reject the tail of the cosmic ray muon velocity distribution;
3. energy of at least 10 MeV is required to be deposited in each of the two scintillator planes in order to exclude accidental radioactive coincidences; and
4. the velocity is further restricted to the region corresponding to this minimum energy, $\beta > 1.2 \times 10^{-3}$.

A total of 158 events survive these cuts, of which 67 are from sample 1 and 91 from sample 2. They are divided into two groups depending upon their apparent velocity: $1.2 \times 10^{-3} < \beta < 5 \times 10^{-3}$ (32 candidates) and $5 \times 10^{-3} < \beta < 10^{-1}$ (126 candidates).

The trajectory of an ionizing particle crossing the MACRO detector is normally well defined by the streamer tube system, which allows for the rejection of corner-clipping events. In this preliminary evaluation of the scintillator response, however, it is useful to apply weaker selection criteria. Streamer tube tracking is not therefore required; instead, a minimum scintillator pathlength assumption of 15 cm is made. Typical cosmic ray muon pathlengths are greater than this value, but it is nevertheless possible that this assumption could cause a monopole candidate with a short scintillator exposure to be rejected. This effect has been included in the calculation of detector acceptance.

5.1.2. PHRASE candidates $1.2 \times 10^{-3} < \beta < 5 \times 10^{-3}$

Monopole candidates in the range $1.2 \times 10^{-3} < \beta < 5 \times 10^{-3}$ are evaluated on the basis of their WFD pulse width. For each, an expected scintillator transit time is calculated from the apparent velocity and the assumed 15 cm pathlength. The resultant range, 100–500 ns, is large compared to both the PHRASE WFD sampling time of 10 ns and the typical muon pulse width of ≈ 35 ns. The expected energy deposition in this region is also large, approximately 10–30 times the typical muon level of ≈ 30 MeV. Thus these candidates are expected to produce wide PHRASE WFD pulses which are well over threshold and which can be tested for consistency with the expected scintillator transit time.

The PHRASE WFD pulse width resolution is ≈ 4 ns, based upon an assumed uniform distribution of actual event times within the 10 ns sampling window. Hits which appear in up to three adjacent scintillation counters are summed under the assumption that they represent separate segments of a single particle track. In no case is the observed total pulse width consistent with the expected crossing time (Fig. 11). All candidates are therefore rejected from the range $1.2 \times 10^{-3} < \beta < 5 \times 10^{-3}$.

5.1.3. PHRASE candidates: $5 \times 10^{-3} < \beta < 10^{-1}$

Monopoles with velocities in the range $5 \times 10^{-3} < \beta < 10^{-1}$ are expected to produce scintillation light at a rate 30–60 times that of a minimum

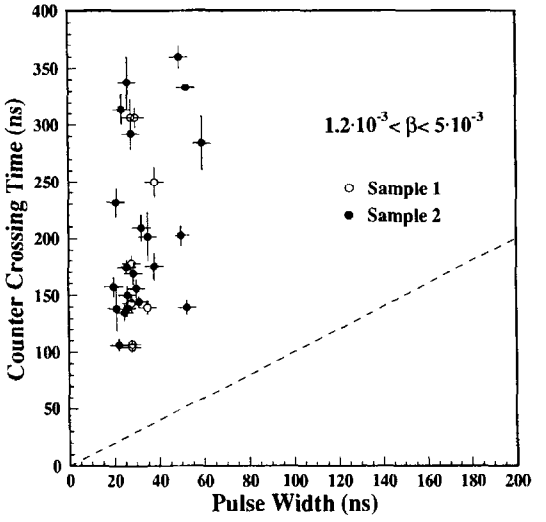

Fig. 11. Calculated counter crossing time versus pulse width for PHRASE candidates in the range $1.2\times10^{-3} < \beta < 5\times10^{-3}$. The diagonal line indicates the minimum pulse width expected for the assumed pathlength of 15 cm. No candidates meet or exceed this expectation.

ionizing particle. Because the expected counter crossing times (6–120 ns) are comparable to cosmic ray muon pulse widths, however, and because the PHRASE flash ADC's saturate for pulses in the muon energy range and above, such monopoles could be confused with cosmic ray muons. Discrimination among these events, then, must be made on the basis of energy deposition. As with the pulse width analysis, hits which appear in up to three adjacent counters are summed.

The measured energy loss is converted into visible light density by assuming a fixed 15 cm pathlength in the scintillator. The result is compared to the prediction for monopoles in Fig. 12. A global 95% confidence level upper limit on the energy loss rate of any single event is also shown. All the candidates exhibit energy losses far below those expected for monopoles of the same apparent velocity and so all are rejected.

5.1.4. The PHRASE reflection-based analysis

Analysis of the $5\times10^{-3} < \beta < 10^{-1}$ candidates can also be performed using optical pulse reflections (Section 4.5). This method has different systematic errors than the integrated pulse height approach and so provides a semi-independent check. Each candidate is associated with four waveforms: two from the two ends of the scintillation counter(s) struck in the first plane and two from the two ends of the counter(s) struck in the second plane. The time region corresponding to the first few optical reflections is known for each waveform, and an energy analysis is performed by comparing the unsaturated (linear) regions of the main photomultiplier pulse to those of the optical reflections. Depending on the position of the event along the counter, the tail of the main pulse may overlap with the first reflection; as we do not correct for this effect it may lead to an overestimate of the energy deposition. If the overlap is significant, however, the pulse from the other end or the second (third, etc.) optical reflections are used instead.

5.1.5. Categorizing the rejected PHRASE candidates

While streamer tube tracks are not required by the PHRASE analysis, they are nonetheless available for a subsample of the rejected events and so are used to help categorize them. In the particular case of the

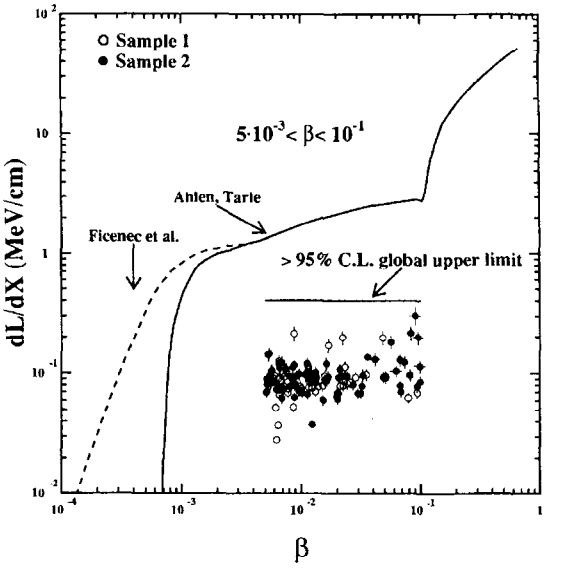

Fig. 12. Energy loss versus velocity for PHRASE events in the range $5\times10^{-3} < \beta < 10^{-1}$. The calculated monopole energy loss rates from [9,18] are also given, as is a 95% confidence level upper limit on the maximum energy loss of any single individual candidate. In no case is the energy deposition of a candidate consistent with that expected for a monopole of the same apparent velocity.

downward-going tracks, the available data are consistent with the hypothesis of a single cosmic ray muon that passes through one scintillator plane but stops just before reaching a second. The two-plane requirement is satisfied by subsequent muon decay, which produces an electron in the second plane. In support of this hypothesis the energy loss spectrum in the apparent entry plane is of the Landau type, while the spectrum in the second plane is flatter and has a cutoff at 50 MeV. The time delay between the hits in the first and second planes, furthermore, is consistent with the decay of a particle with lifetime on the order of a few μs (Fig. 13).

Streamer tube tracking information is also available for many of the apparently upward-going (negative β) events. In each of these cases complete tracks are observed in the streamer tubes, but they include only one of the two triggered scintillation counters. The second is separated from the track. This is consistent with the hypothesis of a (downward-going) cosmic ray muon which strikes an inactive region in one of the two scintillator planes, but meets the PHRASE two-plane requirement by coincidence with a natural radioactive decay. The apparent velocity of these events is randomly determined by the relative timing of the muon and radioactive decay pulses and they sometimes populate the region of interest.

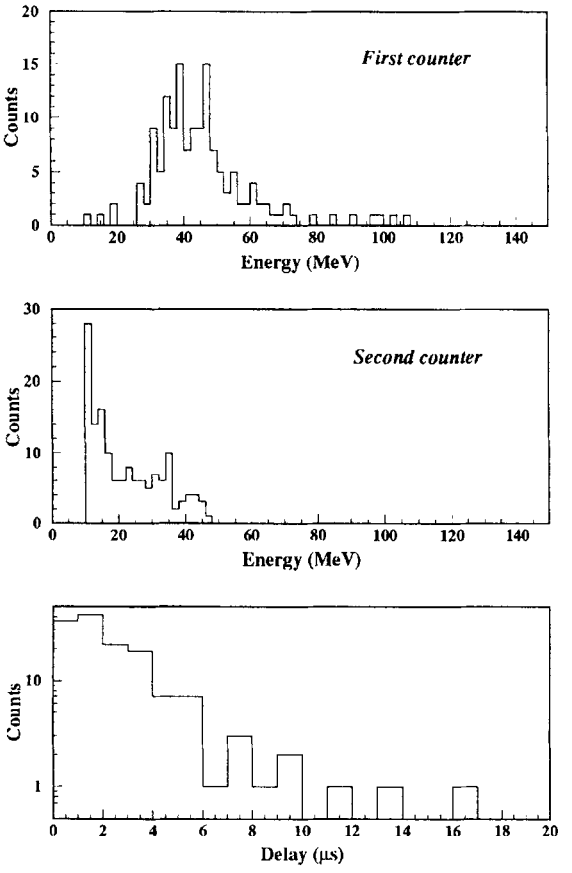

Fig. 13. Energy loss and timing measurements for the downward-going PHRASE candidates. Losses in the first scintillator counter are consistent with the Landau distribution for minimum ionizing particles, while in the second counter there is a cutoff at ≈ 50 MeV. The timing distribution (the delay between the first and second counters signals) is consistent with a few μs lifetime particle decay.

5.2. The ERP analysis

The ERP monopole analysis applies to velocities in the range $10^{-1} < \beta < 1$. Data were acquired during the period December 1992 to July 1993, during which the entire lower MACRO detector was operational, excluding only the north and south faces. The total exposure of 5.3×10^{14} cm^2 s sr included 4.7 million ERP muon triggers, of which 2.7 million included two or more scintillator planes.

5.2.1. ERP Event selection

A fixed scintillator pathlength is assumed in the ERP analysis for the same reasons it is adopted by the PHRASE (Section 5.1.1). In the case of the ERP, however, 10 cm rather than 15 cm is used. The difference partially reflects the fact that the ERP is a single-counter analysis, while the PHRASE study sums up to three adjacent signals. This allows the ERP to discriminate against muon-induced electromagnetic showers which are not as relevant to the PHRASE analysis because it does not include the $\beta > 10^{-1}$ regime. As with the PHRASE, the loss of acceptance due to the fixed-pathlength assumption is included in the exposure calculation.

The ERP analysis requires triggers in two separate scintillator planes and defines those two counters with the highest recorded energy deposition at each end of the candidate 'track' as the primary and secondary counters. The following event selections are then made:

1. The primary and secondary counters must be separated in the vertical direction by at least 2 m,

insuring a time of flight long enough for accurate velocity measurements;

2. the total energy deposition in each of the primary and secondary counters must be at least 600 MeV, ≈ 3 times less than that expected for monopoles of velocity $\beta = 10^{-1}$ with 10 cm pathlength in the scintillator;
3. the 2 V dynamic range of the WFD must be saturated in both the primary and secondary counters, as is expected for monopole candidates in this velocity range (the muon-induced electromagnetic shower background, which can generate large integrated pulse heights through well-distributed individual pulses, does not necessarily satisfy this requirement); and, finally,
4. while operation of the streamer tube system is not required for the ERP analysis, nevertheless, in those cases were such data are available, both the primary and secondary counters must lie along the same track.

The number of events surviving these requirements is 33. Of these, none exhibits the characteristics of a single, isolated particle crossing; that is, all are to first order consistent with the background of large cosmic ray muon-induced electromagnetic showers. However, we note that in case monopoles are accompanied by showers of relativistic particles, the velocity determination obtained in the described system might be biased. This would affect the sensitivity for fast monopoles in case of a large cross section for proton decay catalysis.

5.2.2. ERP candidate velocity

Each of the 33 remaining events satisfies the aforementioned 600 MeV energy deposition requirement in both the primary and secondary scintillation counters. The value of this threshold, however, is determined on the basis of the lowest velocity in the analysis range, $\beta = 10^{-1}$. In fact, each of the remaining candidates' apparent reconstructed velocities is higher than this, as is the energy deposition expected from them.

Fig. 14 shows the relationship between measured and predicted energy deposition as a function of apparent velocity for the 33 remaining events. None exhibits energy loss consistent with the monopole hypothesis in both the primary and secondary counters, and so all are rejected. One event does saturate the ERP energy calibration (Section 4.4) in the primary counter, in which case only a lower limit of 8 GeV can be assigned. This event is nevertheless rejected along with the rest on the basis that the energy recorded in the secondary counter is much less than that expected for a monopole with the corresponding velocity ($\beta \approx 1$). All 33 rejected candidates exhibit localized detector activity consistent with their categorization as cosmic ray muon-induced electromagnetic showers.

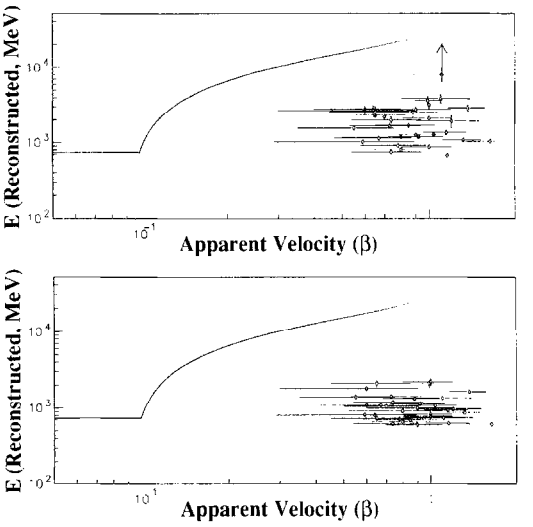

Fig. 14. ERP candidate energy losses in the primary (top) and secondary (bottom) counters. The expected monopole energy loss is from [9]. No candidate exhibits energy loss consistent with the hypothesis of a magnetic monopole in both the primary and secondary counters. The energy deposition of one event is above ERP calibration range in the primary counter (only), for which the arrow indicates a lower limit.

6. Conclusions

The PHRASE- and ERP-based scintillator systems described here are efficient in the search for fast magnetic monopoles in the range $10^{-3} < \beta < 1$. They are a significant part of the full MACRO monopole program and, considering the results already published in [13], they demonstrate the ability of the MACRO liquid scintillator to cover a wide velocity range. These techniques will be also combined with the other detector components in order to provide redundant signature of possible candidates.

The analysis methods described in this paper will serve as reference for our future analyses. They have been tested in order to evaluate the experimental background. Since no candidate was produced in the test period, the present results can be used to establish upper limits on flux of fast magnetic monopoles. Considering the total PHRASE exposure of 5.7×10^{14} cm^2 s sr, applicable to velocities of $1.2 \times 10^{-3} < \beta < 10^{-1}$, and the ERP exposure of 5.3×10^{14} cm^2 s sr, applicable to velocities of $10^{-1} < \beta < 1$, and taking into account the different detector acceptances of the two analyses, the corresponding 90% confidence level upper limits on the isotropic flux of magnetic monopoles are:

$$\Phi < 4.0 \times 10^{-15} \text{ cm}^{-2} \text{ s}^{-1} \text{ sr}^{-1}$$
$$\text{for } 1.2 \times 10^{-3} < \beta < 10^{-1},$$

and

$$\Phi < 4.4 \times 10^{-15} \text{ cm}^{-2} \text{ s}^{-1} \text{ sr}^{-1}$$
$$\text{for } 10^{-1} < \beta < 1.$$

Such results are consistent with those from other monopole analyses [21–23].

Including all MACRO data obtained through July 1995, using various detector subsystems and trigger configurations, sensitivity at the level of the Parker bound [12] can be obtained in the range $10^{-4} < \beta < 1$. It is the long-term goal of the MACRO experiment to extend its sensitivity to well below the Parker bound.

Acknowledgements

We gratefully acknowledge the staff of the *Laboratori Nazionali del Gran Sasso* and the invaluable assistance of the technical staffs of all the participating institutions. For generous financial contributions we thank the U.S. Department of Energy, the National Science Foundation and the Italian *Istituto Nazionale di Fisica Nucleare*, both for direct support and for FAI grants awarded to non-Italian MACRO collaborators.

References

[1] P.A.M. Dirac, Proc. R. Soc. A 133 (1931) 60.
[2] G. 't Hooft, Nucl. Phys. B 79 (1974) 276.
[3] A.M. Polyakov, JEPT. Lett. 20 (1974) 194; J. Preskill, Phys. Rev. Lett. 43 (1979) 1365.
[4] E.W. Kolb and M.S. Turner, The Early Universe (Addison-Wesley Publishing, New York, 1990).
[5] D.E. Groom, Phys. Rep. 140 (1986) 323.
[6] J. Harvey, Monopole '83. Proc. NATO Adv. Res. (Workshop Plenum Press, New York, 1984) p. 137.
[7] S.P. Ahlen, Phys. Rev. D 17 (1978) 229.
[8] S.P. Ahlen and K. Kinoshita, Phys. Rev. D 26 (1982) 2347.
[9] S.P. Ahlen and G. Tarlé, Phys. Rev. D 27 (1983) 688.
[10] S.P. Ahlen et al., (the MACRO Collaboration) Nucl. Inst. Meth. A 324 (1993) 337.
[11] S.P. Ahlen et al., (the MACRO Collaboration) Astropart. Phys. 1 (1992) 11.
[12] E.N. Parker, Appl. J. 163 (1971) 255.
[13] S. Ahlen et al., Phys. Rev. Lett. 72 (1994) 608.
[14] M. Ambrosio et al., Astropart. Phys. 4 (1995) 33.
[15] S. Ahlen et al., Search for Magnetic Monopoles with the MACRO Track-Etch Detector, LNGS-94-115 (1994).
[16] A. Baldini, et al., Nucl. Inst. Meth. A 305 (1991) 475.
[17] J.B. Birks, Proc. Phys. Soc. A 64 (1951) 874.
[18] D.J. Ficenec et al., Phys. Rev. D 36 (1987) 311.
[19] R. Voltz et al., J. Physique 29 (1968) 159 and 297.
[20] F.D. Brooks et al., Nucl. Instr. Meth. 162 (1979) 477.
[21] J.L. Thron et al., Phys. Rev. D 46 (1992) 4846.
[22] S. Orito et al., Phys. Rev. Lett. 66 (1992) 1951.
[23] E.N. Alexeyev et al., Nuovo Cim. Lett. 35 (1982) 413.